FINAL REPORT

FINITE ELEMENT MODELING AND ANALYSIS OF REINFORCED-CONCRETE BRIDGE DECKS

R. Michael Biggs
Graduate Research Assistant

Furman W. Barton, Ph.D., P.E.
Faculty Research Scientist

Jose P. Gomez, Ph.D., P.E.
Senior Research Scientist

Peter J. Massarelli, Ph.D.
Faculty Research Associate

Wallace T. McKeel, Jr., P.E.
Research Manager

Virginia Transportation Research Council
(A Cooperative Organization Sponsored Jointly by the Virginia Department of Transportation and the University of Virginia)

In Cooperation with the U.S. Department of Transportation
Federal Highway Administration

Charlottesville, Virginia

September 2000
VTRC 01-R4

ABSTRACT

Despite its long history, the finite element method continues to be the predominant strategy employed by engineers to conduct structural analysis. A reliable method is needed for analyzing structures made of reinforced concrete, a complex but common ingredient in many bridges in Virginia. As an effective alternative to extensive experimentation, this study was implemented to evaluate the plausibility of finite element analysis of reinforced-concrete bridge decks.

Analytical evaluations were performed with the commercial, general-purpose finite element code ABAQUS, which can effectively depict the nonlinear behavior of concrete. It also has the unique capability of describing the behavior of reinforcing bars independently of the concrete material. Three-dimensional finite element models were developed to determine the overall structural response of several reinforced-concrete systems. Biaxial strain distribution through the element thickness, longitudinal normal girder strains, and displacements were predicted with reasonable accuracy. The accuracy of the model was verified with hand calculations or response data acquired from laboratory testing.

The validated finite element models of the structural systems were used to evaluate the Route 621 Bridge over the Willis River, specifically, the composite action and global response of the reinforced-concrete deck and steel girders. Subsequent phases of this project include parameterization studies of this and future reinforced-concrete bridge models.

FINITE ELEMENT MODELING AND ANALYSIS OF REINFORCED-CONCRETE BRIDGE DECKS

R. Michael Biggs
Graduate Research Assistant

Furman W. Barton, Ph.D., P.E.
Faculty Research Scientist

José P. Gomez, Ph.D., P.E.
Senior Research Scientist

Peter J. Massarelli, Ph.D.
Faculty Research Associate

Wallace T. McKeel, Jr., P.E.
Research Manager

INTRODUCTION

Many bridges built in the past 50 years are composite structures with decks constructed of reinforced concrete and supported by longitudinal steel girders. Because of their normal deterioration, the introduction of new safety standards, and the increasing traffic volume and loads, a high percentage of the older bridges require rehabilitation or expansion. Often, the choice between constructing a new bridge and rehabilitating the existing one must be made. As the recent issue of replacing the Woodrow Wilson Bridge over the Potomac River exemplifies, this choice can be a much debated one (Reed, 1996).

An essential factor in making a sound decision is knowledge of the strength of the bridge in its existing form. Unfortunately, the inelastic response, load distribution characteristics, and ultimate strength of multigirder bridges cannot be realistically assessed by use of simplified procedures currently used in design and evaluation. Prediction of this behavior ultimately requires extensive experimentation or advanced analytical techniques. In many cases, analytical methods are more economical and expedient than laboratory or field testing, and a number of researchers have extolled the potential of using finite element analysis to predict bridge response with reinforced-concrete deck compositions (Ashour & Morley, 1993; Huria, 1993; Mabsout, 1997; Razaqpur, 1990).

The development of commercial finite element codes, which provide a unique program interface with which to analyze a system, has helped practitioners attain a better appreciation for both the usefulness and limitations of finite element modeling of reinforced concrete (Darwin, 1993). Evaluation of specific applications, such as reinforced-concrete bridge decks, can be

handled using these codes. However, to identify possible modeling discrepancies and errors and to verify the accuracy of these computer codes, results from nonlinear finite element analyses need to be compared with those from actual experiments. This may be achieved only if the analysis can account realistically for the material and geometric properties of the various components of a structure and the interaction among them (Chowdhury, 1995).

A definitive technique for analyzing reinforced concrete, one of the most used composite materials in construction, has been difficult to develop. Researchers acknowledge that the finite element method works very well for many structural materials such as steel and aluminum, which have well-defined constitutive properties. When the constitutive behavior is not so straightforward, the task is more difficult. For materials such as concrete, in which discrete cracking occurs, this is certainly the case. The complexity of reinforced concrete is a major factor that limits the capabilities of the finite element method (Chen et al., 1993).

Until recently, only linear models were used to analyze structural systems composed of complex materials such as reinforced concrete. More recently, researchers have employed many variations of the constitutive representations of the concrete component, the reinforcement, and the nature of their interaction. A comprehensive summary by Darwin of 24 finite element model studies of reinforced concrete from 1985 to 1991 illustrates the wide range of options available to perform an accurate analysis (Darwin, 1993). Some of the categories compared are indicated in Table 1, along with the frequency with which each option was used in the studies. This illustrates that a primary technique for analyzing general reinforced-concrete structures has yet to be agreed upon.

Table 1. Research on Reinforced-Concrete Finite Element Modeling

Subject	Options	% of References
Type of model	2-dimensional	88
	3-dimensional	12
Concrete compression	Linear elastic	8
	Nonlinear elastic	80
	Elastoplastic	12
Tension stiffening	Incorporated	67
	Not used	33
Steel representation	Distributed	58
	Discrete	37
	Embedded	5
Crack representation	Fixed orthogonal	29
	Fixed non-orthogonal	37
	Rotating	34
Bond representation	Perfect	63
	Bond slip	37

Cracking of the concrete and yielding of the reinforcement dominate the failure behavior of most reinforced-concrete systems. Cracking is regarded as an extremely important phenomenon that can be studied exclusively (Alfaiate et al., 1997; DeBorst, 1997; Loo & Guan, 1997). Ngo and Scordelis (1967) presented the first finite element analysis of reinforced concrete that included the effect of cracking. Studies that followed attempted to represent discrete cracks that occur during a load cycle, but the need to change the topology of the finite element mesh greatly hindered the speed of the process. More recently, researchers have developed models that automatically generate cracking without redefining the element mesh. These models depict the effect of many small cracks that are "smeared" across the element in a direction perpendicular to the principal tensile stress direction (Darwin, 1993).

All studies of reinforced concrete employ one of three possible strategies for accurately representing the reinforcing steel: smeared, embedded, or discrete. This aspect of modeling has also been the subject of independent investigations as to the advantages of one over the other (Barzegar, 1994; Barzegar & Maddipudi, 1997; Jiang & Mirza, 1997; Kwak & Filippou, 1997; Ramaswamy et al., 1995). Table 1 shows that steel reinforcement was most often represented by a distributed layer using a uniaxial constitutive relationship. Particular interaction characteristics such as the ability of steel to take dowel forces are, therefore, not modeled by this uniaxial material. Along with bond quality and aggregate size, these effects are instead taken into account when the overall interaction behavior of reinforced concrete is described (Hibbitt, Karlsson & Sorensen, Inc. [HKS], 1998a).

The ability of the concrete between cracks to carry stress and provide stiffness in tandem with the reinforcing steel, known as tension stiffening, was first introduced by Scanlon and Murray. They developed models that simulated the loss of stiffness by altering the tensile stress-strain relationship (Scanlon & Murray, 1974; Gilbert & Warner, 1978). Although these early models overestimated the initial cracking load, they produced the closest match with experimental data. The recent incorporation of this concept into commercial finite element codes is based on Hilleborg's 1976 study that combined fracture mechanics of concrete with finite elements and the ability of reinforced concrete to carry stress after cracking (cited in HKS, 1998a).

In addition to studies examining material behavior, several studies have been devoted to assessing the load-carrying capacity and other characteristics of bridges (Azizinamini, 1994; Huria, 1993; Sen et al., 1994; Shahrooz, 1994; Sharooz & Ho, 1998). These investigations provide excellent information because their analytic solutions attempt to explain the behavior that occurs in the field, even at ultimate load.

PURPOSE AND SCOPE

The primary objective of this study was to establish and demonstrate a convenient, reliable, and accurate methodology for analyzing reinforced-concrete structures with particular emphasis on reinforced-concrete bridge decks. A secondary objective was to develop a

capability for predicting stress and strain distribution through the thickness of reinforced-concrete bridge decks. Such information is not easily obtained through experimentation.

A specific objective of the analytical evaluation included the development of a finite element model that could correctly represent global bridge behavior and accurately predict strains, stresses, and displacements in the deck. Dynamic, fatigue, and thermal analyses, although certainly worth investigating in future project phases, were not included in this study.

METHODOLOGY

ABAQUS Version 5.7, a general purpose finite element code developed by HKS, was selected as the basic platform for this study. ABAQUS has a unique procedure for attaining solutions through the entire behavioral regime of reinforced concrete. All subsequent finite element models were developed using ABAQUS.

The next step was to demonstrate how reinforced concrete is modeled within ABAQUS and to validate the results predicted by the ABAQUS models by comparing them with relevant experimental data and accepted design calculations. Examples of reinforced-concrete elements for which experimental data were available, from either previous analyses or laboratory or field tests, were selected. These problems included a simple reinforced-concrete beam, a reinforced-concrete slab, and a composite steel girder with a partial concrete slab. The effectiveness of ABAQUS in analyzing reinforced-concrete beams and slabs also established a basis for its use in modeling a complete bridge deck.

A complete analysis using ABAQUS requires a description of the material, the model configuration, boundary conditions, and loading. For service-load simulations, at least two material constants are required to characterize the linear elastic behavior of the material: Young's modulus (E) and Poisson's ratio (ν). For nonlinear analysis, the steel and concrete uniaxial behaviors beyond the elastic range must be defined to simulate their behavior at higher stresses. The minimum input parameters required to define the concrete material are the uniaxial compression curve, the ratio of biaxial and uniaxial compressive strength, and the uniaxial tensile strength. ABAQUS is equipped with default values if necessary, which are indicative of typical concrete performance (HKS, 1998b).

Boundary conditions that represent structural supports specify values of displacement and rotation variables at appropriate nodes. To facilitate a more economical solution, finite element meshes may also use symmetry, which can be implemented with symmetric boundary conditions. Linear springs may also be considered supports in studies where a component rests on bearing pads. ABAQUS allows the user to define axial spring elements, connected to a node and support that have the appropriate stiffness coefficients.

The reinforced-concrete slabs investigated were modeled with quadrilateral shell elements. ABAQUS can provide response information at the nodes and element stresses at

designated integration points within the element. Stresses at various points through the thickness of the element can also be provided, which is particularly important for this study. Beam elements were used in this study to simulate a typical reinforced-concrete beam and W-shape girders. The user can choose the type of beam element and select the shape of the cross section.

In the case of concrete modeling, ABAQUS employs a plasticity-based constitutive model that simulates cracking, tension stiffening, shear capacity of cracked concrete, and crushing in compression. All types of elements may be used to model concrete in ABAQUS, including the beam and shell elements employed in this study. Figure 1 shows the general type of behavior exhibited by reinforced concrete in tension. The user defines this curve in ABAQUS to simulate the tension stiffening behavior of the concrete elements.

The reinforcing steel is modeled as a one-dimensional element with only uniaxial stiffness properties oriented along its direction in the parent beam or shell element. It is typically defined as individual layers rather than single bars and may be defined singly or embedded in the oriented surface of the concrete. Either way, the definition of the reinforcement's geometry, orientation, and material properties is independent of the definition of the underlying concrete element.

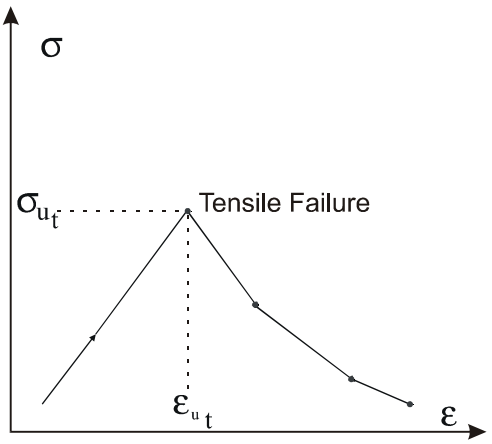

Figure 1. Tension Stiffening Model for Concrete

VERIFICATION STUDIES AND RESULTS

Reinforced-Concrete Beam

The finite element model of a reinforced-concrete beam, simply supported, and subjected to a uniformly distributed load, was initially investigated. The intention of this example was to do the following:

- analyze standard beam elements using plain concrete theory

- combine these elements with one-dimensional strain theory elements for reinforcing steel

- compare finite element results with hand calculations.

The fact that cracking is an important aspect of the general behavior predicates investigating the concept of tension stiffening. Experimenting with this parameter is an important part of model verification.

The beam selected for analysis had a span of 6.1 m (20 ft), a width of 0.25 m (10 in), and a depth of 0.64 m (25 in). The concrete had a strength f'_c of 41.4 MPa (6,000 psi) and a modulus of 30.5 GPa (4,420 ksi). The reinforcing steel had a modulus of 200 GPa (29,000 ksi), a yield stress of 414 MPa (60 ksi), and an area of 1530 mm^2 (2.37 in^2). The loading was a uniform load of 62.2 kN/m (4,260 lb/ft), which is close to the ultimate load of the beam. This load was applied incrementally to facilitate solution convergence. Maximum stresses attributable to the applied load were calculated in accordance with the code of the American Concrete Institute. A finite element model of the beam, consisting of 20 elements, was also developed, and stresses and deflections were determined. The appropriate properties of concrete and steel, including tension stiffening, were included in the model input.

Figure 2 shows the deflection of the entire span, as calculated by the model and by traditional hand calculations. Figure 3 shows the compressive stress in the top fiber of the beam as calculated by the model and by hand. As expected, the maximum stress is at the midspan, and the finite element model shows excellent correlation with the hand calculation. Figure 4 shows the stress in the reinforcing steel. The finite element model again matches the maximum stress at midspan calculated by hand. However, the curve is not a smooth, nonlinear curve such as the one predicted by the hand calculations. Instead, the steel carries very little stress in the elements that extend approximately 1 m (3.3 ft) out from the support. As may be seen from the figure, the reinforcement stress does not conform to the hand calculation curve in the vicinity of the support. This difference is likely attributable to the definition of tension stiffening in the model that could predict more severe cracking near the ends of the model.

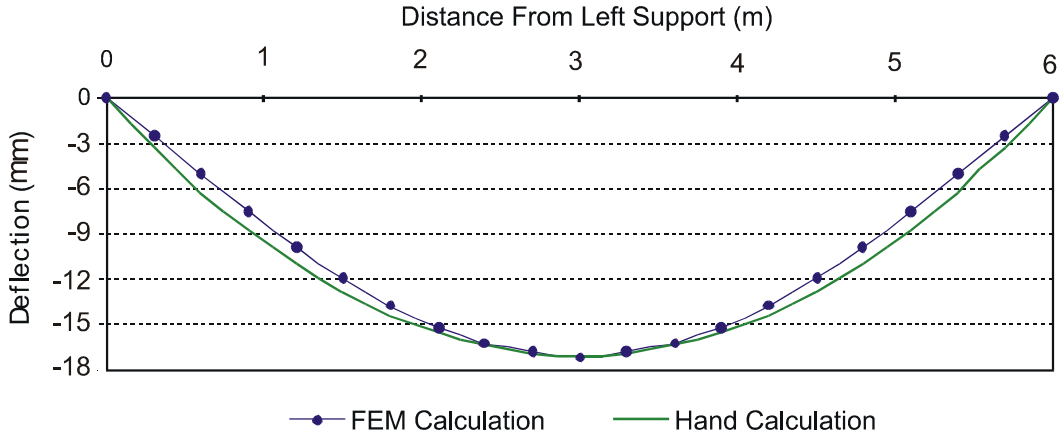

Figure 2. Deflection Across Span

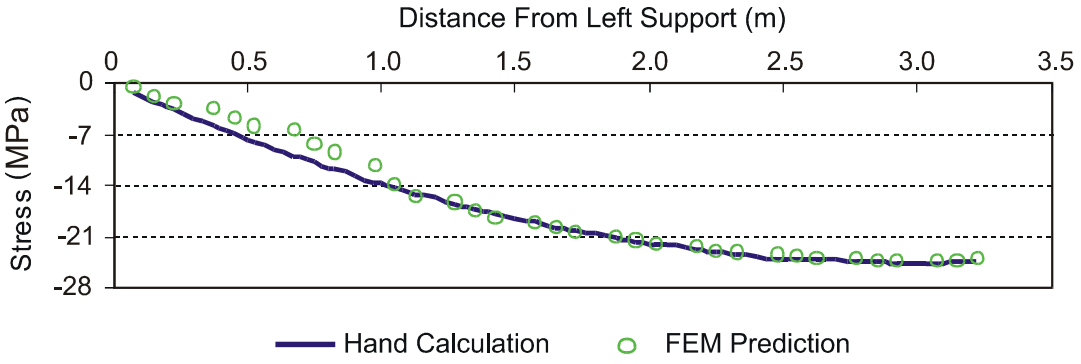

Figure 3. Compressive Stress in Top Fiber of Beam

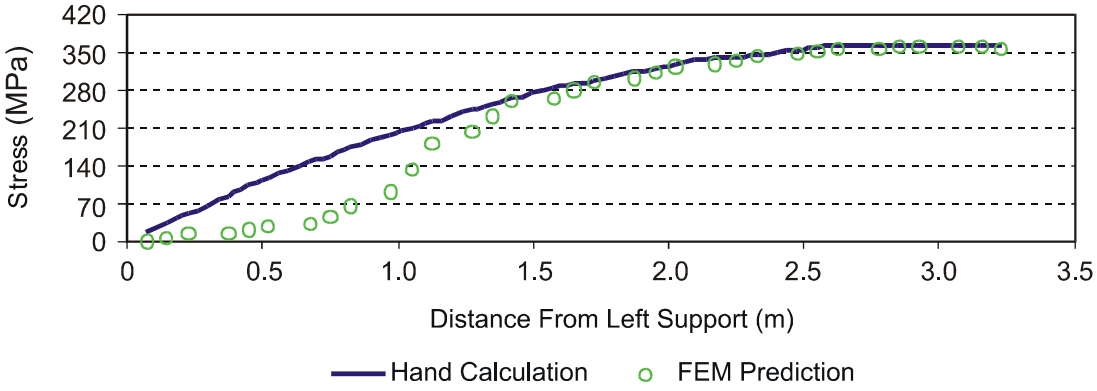

Figure 4. Steel Reinforcement Stress Along Beam

Reinforced-Concrete Slab

Further verification of the validity of finite element models of reinforced-concrete components may be demonstrated by comparing the predicted response of the model with experimental results obtained from laboratory tests of a two-way reinforced, simply supported concrete slab (Graddy et al., 1995). Load deflection behavior, stress distribution, and crack initiation, three important results obtained from the model, were compared to values for similar behavior obtained for the experimental specimen. The success of this analytical model will serve as a precursor to subsequent research of bridge deck analysis.

The reinforced-concrete slab tested had a length of 2.13 m (7 ft), a width of 1.83 m (6 ft), and a thickness of 191 mm (7.5 in). It was reinforced in both the top and bottom of the slab. The properties of the concrete and reinforcing steel were the same as those used in the previous simple beam example. The cast-in-place test slab was simply supported at its edges on neoprene bearing strips represented in the finite element model by linear springs having equivalent stiffness properties. Strain gages were attached to both the top and bottom reinforcement in the longitudinal and transverse directions. Concrete strain gages were also attached to the top and bottom surfaces of the slab at the same locations. Deflections were measured at the edges, just inboard of the supports, and at the center. The net deflection at the center was obtained by averaging the edge displacements and subtracting it from the measured center deflection.

Loading was applied monotonically over an area 406 by 610 mm (16 by 24 in) in the center of the slab. Additional details of the reinforcement, instrumentation, and loading may found in Graddy et al. (1995).

Model Characteristics

Because the slab had two axes of symmetry, it was possible to represent the full slab by modeling only one fourth of the slab. The model contained 432 elements, 378 of which were used to represent the slab and 54 the reinforcement. The shell elements representing the slab were 50.8 by 50.8 mm (2 by 2 in) quadrilateral shell elements with four nodes and six degrees of freedom per node. This resulted in a slab model with 418 nodes and 2,508 degrees of freedom. A sketch of the finite element model of one fourth of the slab is shown in Figure 5. The element numbers are shown, and the locations of the longitudinal and transverse strain gages in the test slab correspond to the location of element 132.

Tabular data were used to define the stress-strain behavior of plain concrete in uniaxial compression beyond the elastic range. The first value of compressive stress, usually taken as $0.45f'_c$, which initiates inelastic behavior, is paired with a plastic strain of zero. Several values of stress were extrapolated from a typical stress-strain curve for 41.4 MPa (6,000 psi) concrete. These engineering strain values were converted to plastic strain through subtracting each from the engineering strain at the initiation of inelastic behavior.

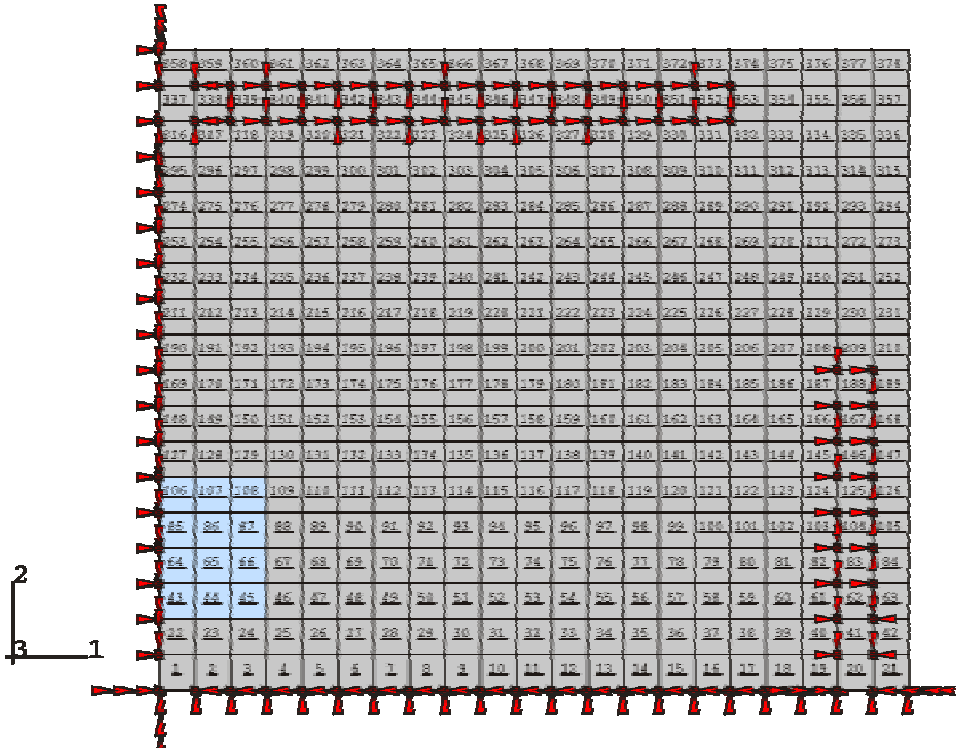

Figure 5. Plan View of Model of Reinforced-Concrete Slab

The load was applied in small increments to overcome difficulties associated with obtaining solutions during unstable response, such as when the concrete cracks. The initial load magnitude was 5% of the maximum applied load of 489.3 kN (110 kips), and the load was then incremented automatically.

The concrete-reinforcement interaction and the energy release at cracking were represented in the model by the use of tension stiffening. In this example, by using several different values for the strain beyond failure, different values of tension stiffening could be included. This illustrates the effect of the parameter effect on the ability of the model to reach convergence and its importance in calibrating the model to a valid experiment.

Deflections were obtained from the node representing the center of the slab. The concrete and steel stresses were obtained at locations corresponding to locations of the strain gages.

Results

The plots in Figure 6 illustrate the effect of tension stiffening on the load deflection response. The values of tension stiffening in the plot ranged from 1.5×10^{-3} to 3.0×10^{-3}. The model with the lowest value of tension stiffening failed to converge to a solution beyond a load of 355.8 kN (80 kips). Specifying this unreasonably low value causes local cracking failure in the concrete, which results in unstable behavior of the overall response. Increasing the tension stiffening to 3.0×10^{-3} makes it easier to obtain numerical solutions without an inordinate amount of computation time or loss in accuracy.

Although the measured and predicted displacement behaviors were quite similar, there were discrepancies that were most likely attributable to the test setup. Graddy et al. (1995) calculated a net-center deflection by averaging both edge deflections and subtracting the result from the center deflection. However, problems in the test setup or with warping affect the data when the slab is initially loaded. Data provided by the researchers, and subsequently used for this comparison, showed a considerable difference in the two edge deflections. The data indicated that edge deflections at loads below 89 kN (20 kips) were actually greater than

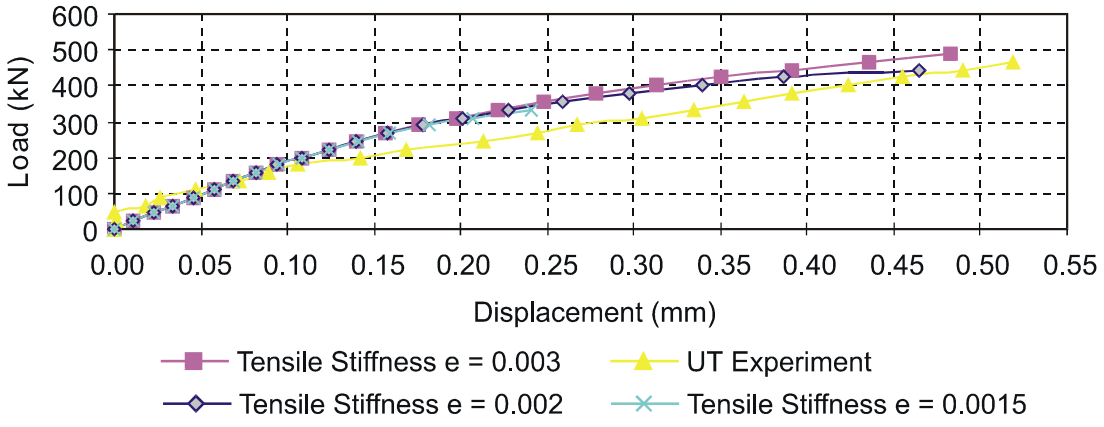

Figure 6. Effect of Tension Stiffening on Response of Model

center deflection. Neglecting the effects of the edge deflection improves the model's match with the present finite element model.

The study also reported that flexural cracking was first observed at a load of about 80 kN (18 kips). These cracks propagated laterally in the *X* and *Y* directions as the applied load increased, with wider cracks occurring parallel with the *X* direction. The finite element model indicated initial cracking at 80 kN (18 kips) as well.

Figure 7 shows the analytical predictions of concrete stress at the top and bottom surfaces of the slab in both the longitudinal and transverse directions at locations corresponding to the location of the strain gages. These analytical results predicted a maximum longitudinal compressive stress in the top approaching 27.6 MPa (4 ksi). The maximum measured compressive stress was reported to be 28.9 MPa (4.2 ksi). However, the maximum transverse compressive stress predicted by the model was approximately 13.8 MPa (2 ksi), and the measured maximum transverse compressive stress was approximately 20.3 MPa (2.9 ksi).

Figure 8 shows the axial stress in the longitudinal reinforcing steel as predicted by the model at a location corresponding to the strain gage locations in the slab. The top layer of steel has predominantly compressive stresses, whereas the bottom layer carries tensile stresses. The tensile stress increases rapidly in the bottom layer above approximately 200 kN (45 kips), indicating that the steel begins to carry a higher percentage of stress once the concrete cracks. As the load increases, there is a gradual movement of the element neutral axis away from the bottom layer of steel and the axial stress becomes increasingly tensile.

These finite element results differ markedly from the experimental results reported in the study by Graddy et al. (1995). Not only does the bottom layer of steel have a much higher state of tensile stress, but the top layers also have tensile stress. This discrepancy is likely attributable to the shifting of the neutral axis, which is a function of cracking in the concrete.

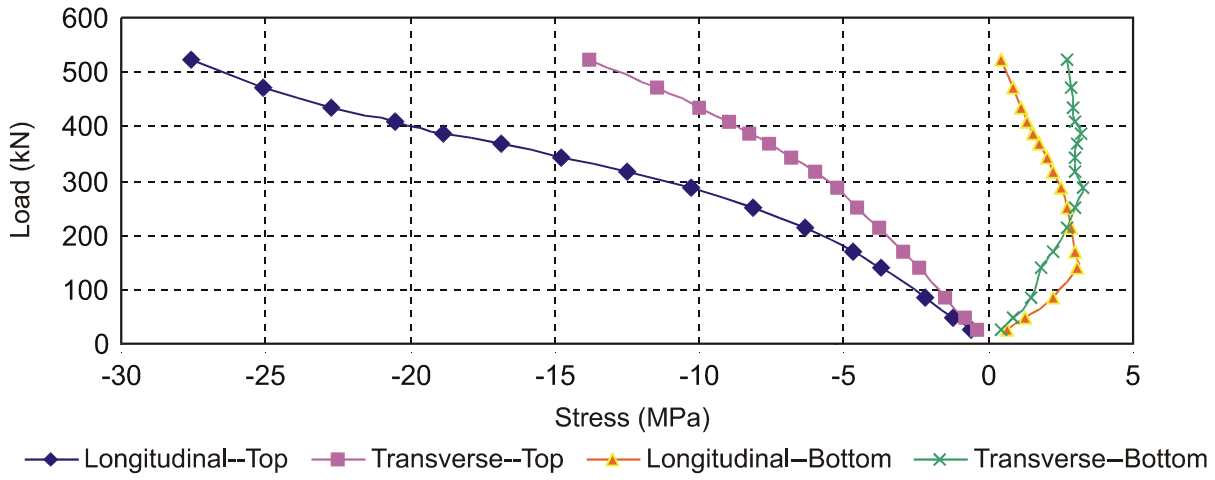

Figure 7. Analytical Stresses for Top and Bottom Concrete Surfaces

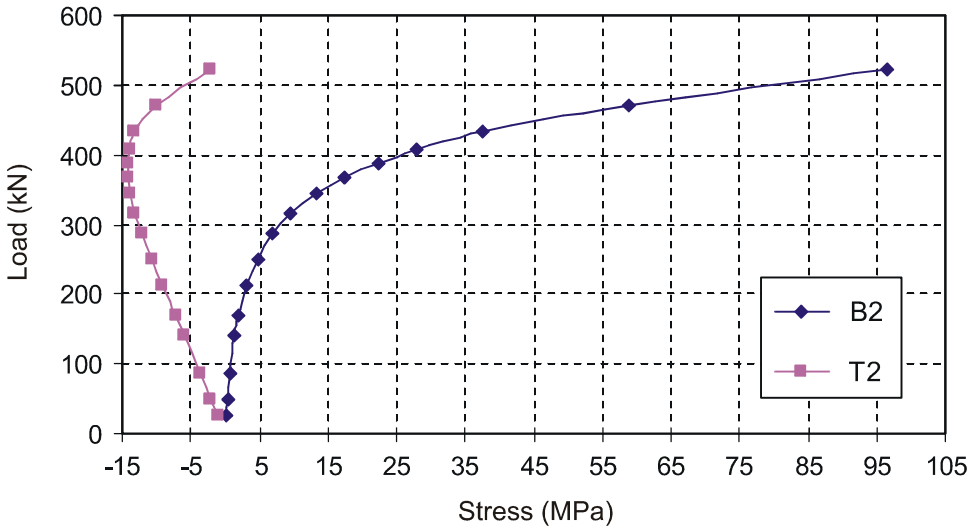

Figure 8. Analytical Results for Steel Stresses

Composite Beam System

For purposes of comparing an isolated composite girder system analyzed with ABAQUS and hand design calculations, one may consider the simply supported slab and girder model shown in Figure 9. The span of the beam is 12.2 m (40 ft), and the spacing between girders

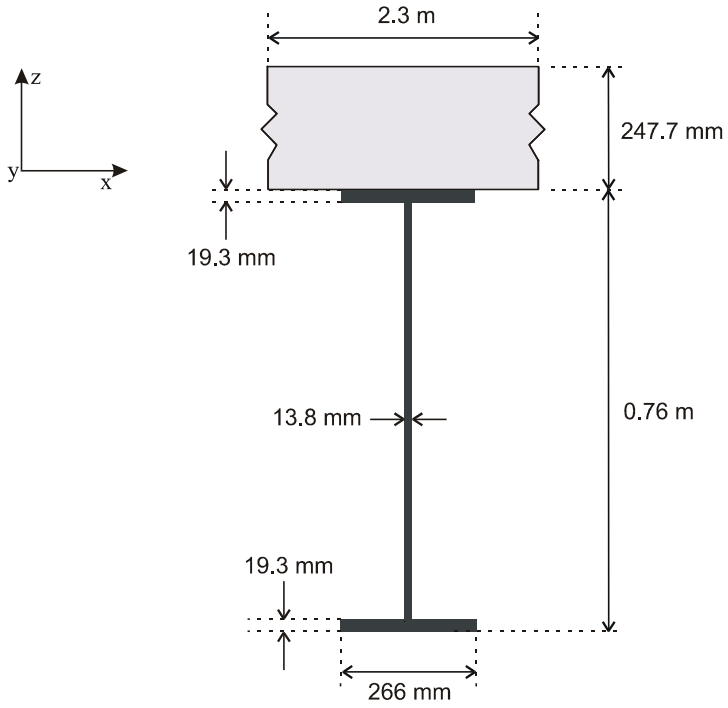

Figure 9. Cross Section of Composite System

is 2.29 m (7.5 ft); thus, the effective flange width is the smaller of one eighth of the span or one half the girder spacing. The dimensions of the model are given in the figure. The steel girder has a yield stress of 248 MPa (36 ksi), and the ultimate strength of the concrete is 27.6 MPa (4 ksi). The beam is subjected to a uniformly distributed static load of 0.012 MPa (1.74 psi) applied to the surface of the slab.

The location of the composite neutral axis was calculated to be 78.5 cm (30.9 in) measured from the bottom flange of the girder, which is 2.62 cm (1.03 in) into the bottom face of the concrete slab. The moment of inertia of the transformed section was determined to be 635×10^3 cm^4 (15.26×10^3 in^4), and the maximum moment attributable to the uniform service load was calculated to be 502.71 kN-m (737.4 ft-lb).

Model Characteristics

The original finite element mesh consisted of 110 elements, 22 rows of 4 concrete deck elements laid on top of 22 girder elements. The initial dimensions of the 247.7-mm-thick (9.75 in) deck elements were 571.5×571.5 mm (22.5×22.5 in). The shell elements (S4R) incorporate thick shell theory for this particular model. The three-dimensional, first order, B31OS beam element represented the girder elements. The nodes defining the two ends of the beam were simply supported.

Element stresses and strains were requested from the top flange, middle web, and bottom flange of the girder element. This output was calculated at the element integration point, which is at the midpoint for this two-node, linear interpolation element. Deck and girder connectivity was achieved in the model by employing multipoint constraints.

Results

Results from the finite element models were used to evaluate some of the important characteristics of bridge behavior and compare them with those calculated by hand. These characteristics included:

- biaxial stress and strain distribution in the deck
- composite behavior of the deck and girder
- load transfer attributable to longitudinal and transverse bending.

The maximum deflection at midspan attributable to the applied load was calculated by hand to be 6.12 mm (0.24 in); the finite element model predicted a maximum deflection of 6.54 mm (0.26 in). Stresses and strains were calculated at six locations, three in the slab and three in the girder. The three points in the concrete slab are the top and bottom surfaces and at its local neutral axis. The three points in the girder are the top and bottom flange (intersecting with the

web) and at its local neutral axis. The results for the concrete deck are listed in Table 2, and for the steel girder in Table 3. The finite element model's calculation of longitudinal stress and strain matched very well with the results calculated by hand.

When the ratio of the stress to the strain at a particular point on the slab was calculated in the finite element model, it differed by about 20% from the ratio calculated by hand. As an example, the ratio between the stress and strain at the bottom of the concrete was only about 3.5, whereas the ratio of the same values in the hand solution was 4.4. Further examination indicated that transverse bending in the slab-girder component, as predicted by the finite element results, contributed to this difference. For example, in the finite element model, there was a state of two-dimensional stress, whereas typical design calculations incorporate equations for only one-dimensional stresses.

The results showed that most of the concrete carries the compressive stress, whereas the entire girder carries the tensile stress with the transition point located at the composite neutral axis, just above the bottom of the concrete slab.

Table 2. Composite Beam Stress and Strain in the Concrete

Parameter	Location	Hand	FEM	
			Longitudinal	Transverse
Stress (MPa)	Top	-2.661	-2.654	0.468
	Middle	-1.173	-1.168	0.025
	Bottom	0.314	0.318	-0.417
Strain ($\times 10^{-6}$)	Top	-87.66	-89.72	28.52
	Middle	-38.65	-38.60	6.60
	Bottom	10.35	12.52	-15.32
Deflection (cm)	Midspan	0.612	0.654	

Table 3. Composite Beam Stress and Strain in the Girder

Parameter	Location	Hand	FEM Longitudinal
Stress (MPa)	Top	2.072	2.652
	Middle	32.120	32.023
	Bottom	62.169	61.396
Strain ($\times 10^{-6}$)	Top	10.35	13.254
	Middle	160.5	160.04
	Bottom	310.7	306.83

FINITE ELEMENT MODEL OF ACTUAL BRIDGE

The researchers developed a complete model of a typical steel girder bridge with a reinforced-concrete deck by employing all of the finite element strategies discussed in earlier sections. The features involved included the following:

- concrete elements
- reinforcing steel
- composite construction
- capability to model deck cracking
- capability to model nonlinear behavior
- capability to conduct static and dynamic analysis.

Despite the fact that experimental data were not yet available for comparison, it was useful to complete a model and conduct a detailed analysis for such a configuration.

Description of Bridge

The structure selected for this demonstration was a three-span continuous bridge carrying Route 621 over the Willis River in Buckingham County, Virginia. Each span has a length of 12.2 m (40 ft) and a width of 7.98 m (26.2 ft). The doubly reinforced concrete deck is supported by four steel girders with a spacing of 2.29 m (7.5 ft). For convenience, the girders were labeled A through D. Figure 10 shows a plan view of the deck, which details general dimensions and the spacing of the girders. The spans from right to left are labeled A through C. The cast-in-place deck, made of Type A4 (27.6 MPa or 4 ksi) concrete, had longitudinal and transverse reinforcement in both the top and bottom.

Figure 11 shows the cross section of the bridge, including the girders, diaphragms, and parapets. The rolled girders have a depth of 758 mm (29.8 in), a web thickness of 14 mm (0.55 in), a flange thickness of 19 mm (0.75 in), and a flange width of 266 mm (10.5 in). The top flanges of the girders are connected to the reinforced-concrete deck with shear studs. Diaphragms, consisting of channel sections 380 mm (15 in) deep, connect between the girders in each span. Diaphragms are located at midspan and adjacent to each support. Parapets, located on either side of the roadway, are constructed of cast-in-place concrete and are fastened to the reinforced concrete with steel bars encased in a stainless steel tube.

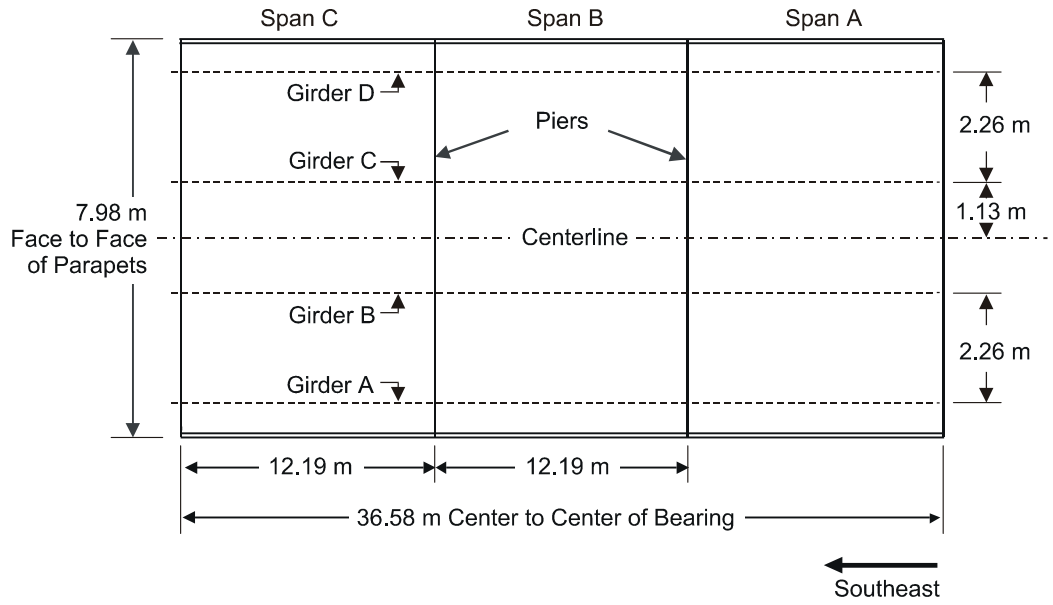

Figure 10. Plan View of Bridge

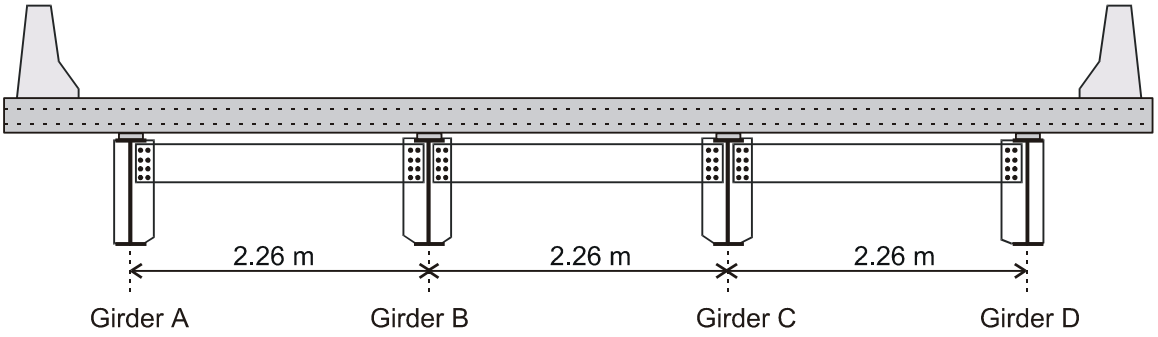

Figure 11. Cross Section of Bridge

Model Characteristics

Several assumptions were made to simplify model development without any loss in the accuracy of the representation. The 1.4% deck gradient was neglected, making the mesh representing the deck parallel with the *X*-*Y* plane. An average deck thickness of 248 mm (9.75 in) was used, and the steel placement through the deck remained constant. The 38-mm (1.5-in) concrete haunch that protects the shear connectors, and separates the girders from the bottom surface of the deck, was not included in the model. The bolted connection between the diaphragms and the girders essentially creates a fixed connection and may be modeled as a node-to-node connection. External components of the bridge that are mechanically connected to the deck are attached in the finite element model by using multipoint constraints.

With these assumptions in mind, the components of the bridge were represented by the following finite element strategies:

reinforced-concrete deck	→	shell elements and rebar elements
steel girders	→	beam elements
diaphragms	→	truss elements
parapets	→	beam elements
interaction	→	simple supports or multipoint constraints
static load	→	surface pressure loads

The complete model had 5,211 elements, separated into 4,320 shell elements, 576 beam elements constituting the girders, 288 beam elements forming the parapets, and 27 truss elements. This resulted in a system with 40,000 total degrees of freedom.

Deck elements were modeled with S4R shell elements. The geometry of the deck was such that the element dimensions were approximately 290 mm (11.4 in) in the transverse direction and 254 mm (10 in) in the longitudinal direction. The transverse dimension was varied slightly to ensure that nodes in the deck mesh were aligned with the girder nodes. With a total bridge length of 36.58 m (120 ft) and a total width of 7.98 m (26.2 ft), the mesh representing the deck consisted of 28 rows of 144 elements.

The steel girders, defined as beam elements, were positioned on a separate plane of nodes parallel with the deck. The girder nodes were defined by copying a nodal layer of the deck to a new plane. This allowed the coordinates of girder nodes to be in line with the deck's nodal layer. This sort of alignment, which occurred for all four pairs of girder and deck nodes, was necessary to provide the proper connectivity between the two layers of elements. Each girder was represented by 144 beam elements, each 254 mm (10 in) in length. Truss elements were used in the finite element model to represent diaphragms, and the parapets were defined in the bridge models as general beam elements. The area, moments of inertia, and torsional rigidity were calculated from geometric quantities of the parapets. The parapet nodes were 295.1 mm (11.6 in) above the deck's nodal layer corresponding to the location of the centroid of the parapet cross section.

Loading

The applied loading consisted of pressure loads applied to deck elements. The load magnitudes corresponded to the tire loads of a standard AASHTO-type, multiaxle truck, and the load location corresponded to the tire footprints. Based on truck weights used in an earlier field test (Misch, 1998), the researchers assumed that the total truck weight was 247.3 kN (55.6 kips). The total load was distributed such that the truck's front axle carried 25% of the gross weight and the two rear axles carried the remaining 75% of the weight. The appropriate dimensions and location of each tire patch and the total gross weight applied are illustrated in Figure 12. The actual location of the load on the bridge was applied to an arbitrarily chosen region of Span A. Figure 13 illustrates the model of the complete span, which includes the deck, parapets, girders, and diaphragms.

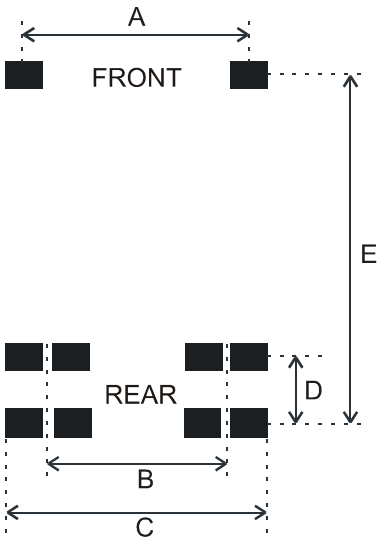

Truck	Dim. A (m)	Dim. B (m)	Dim. C (m)	Dim. D (m)	Dim. E (m)	Total Weight (kN)
(No. 58138)	2.06	1.83	2.36	1.35	5.87	247.3

Figure 12. Characteristics of Applied Load

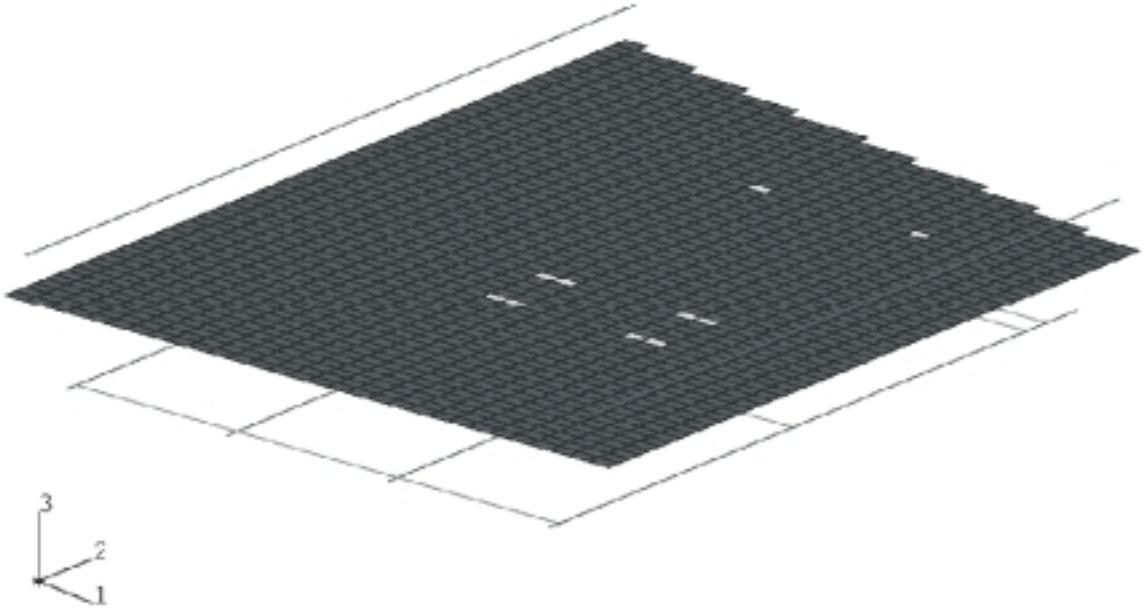

Figure 13. View of Span A and Location of Applied Load

Results

The following data are applicable only to the first span, Span A, which extends from the abutment to the first pier. Longitudinal and transverse stresses in the girder and deck are presented at particular locations. The data show the global behavior of the bridge model, particularly the distribution of compressive and tensile stresses in the deck.

Figure 14 shows the deflection pattern in Span A as a result of the load applied to the bridge model. As expected, the area of the bridge under the rear axles of the truck load sustained the maximum deflections. This area supported 75% of the gross load. The maximum deflection was approximately 0.9 mm (0.04 in) at girder node 2723. With reference to Figure 12, this location is approximately halfway between the front and rear axles and is located at Girder C.

Figures 15 and 16 show contours of the transverse strain distribution in the reinforced-concrete deck. In Figure 15, the transverse compressive strain in the top fiber of the deck is most evident directly under the rear-axle load patch. The plot of transverse strain in the bottom fiber of the slab, shown in Figure 16, indicates the tensile behavior of the deck attributable to the load. The section of the deck directly over the girder, between the rear axle loads, has a tensile strain of about 3 microstrain, whereas the strain in the bottom part of the deck directly under the load is approximately 30 microstrain.

Figures 17 and 18, respectively, show the compressive and tensile strain distributions across the transverse strip. Finally, a plot of the longitudinal tensile strain in Girder C, along a line extending from the abutment to approximately the midpoint of the bridge, is shown in Figure 19. As evident from the figure, the portion of Girder C directly underneath the rear axle load patch has the highest tensile strain. The level of strain then decreases until it becomes compressive over the pier support and then becomes negligible in Spans B and C. This observation confirms the expected response of the girder in the vicinity of the load.

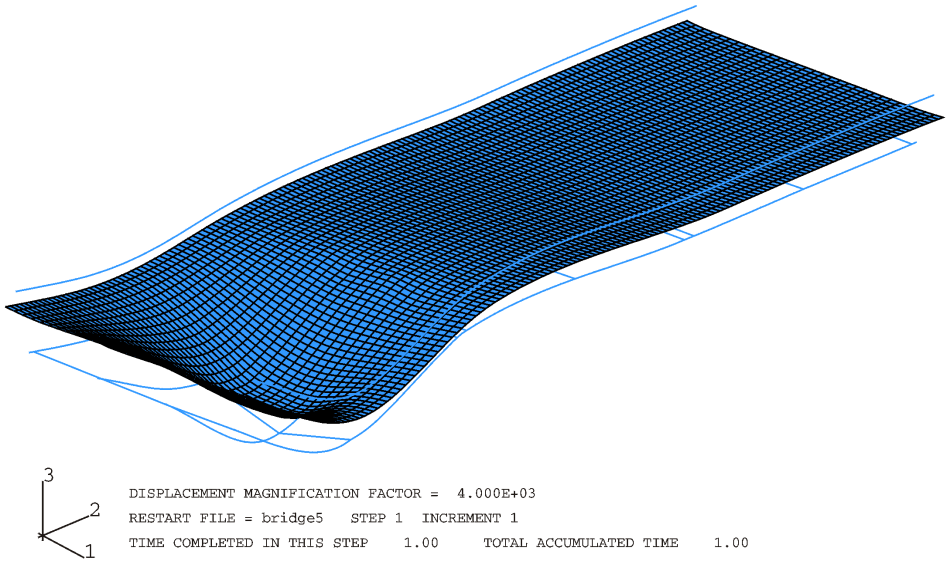

Figure 14. Deflection of Span A Attributable to Static Truck Load

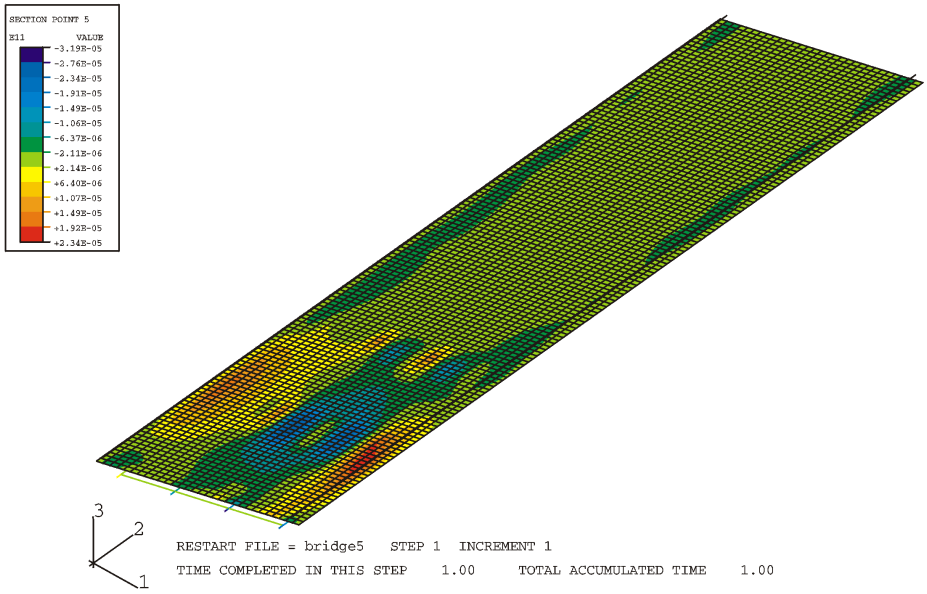

Figure 15. Transverse Strain at Top Surface of Deck

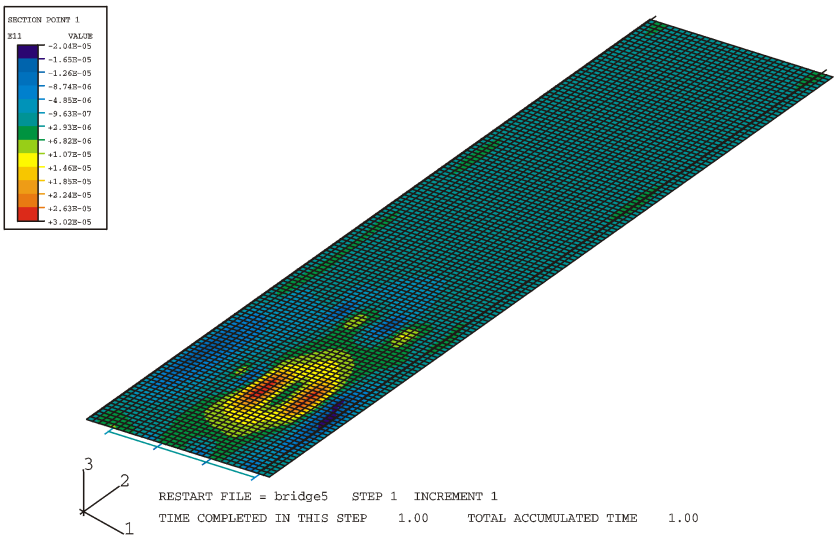

Figure 16. Transverse Strain at Bottom Surface of Deck

Figure 17. Compressive Strain Distribution Across Transverse Strip

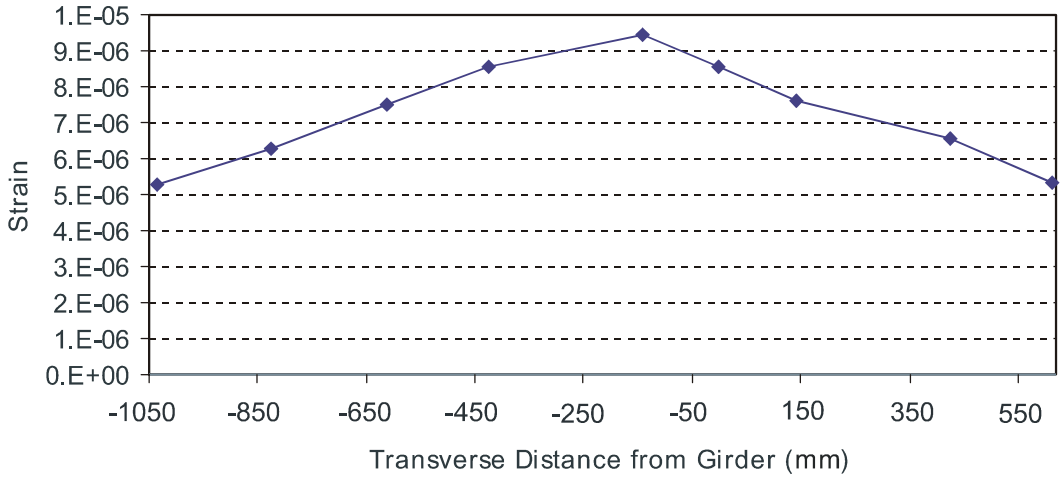

Figure 18. Tensile Strain Distribution Across Transverse Strip

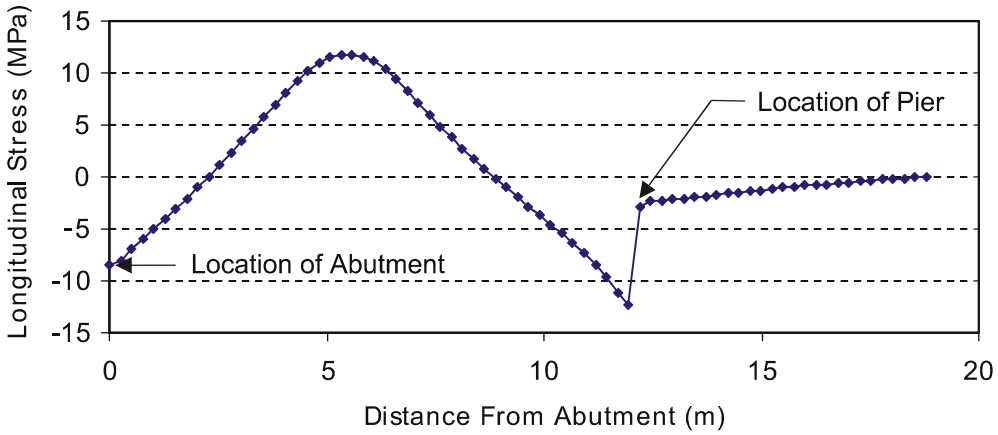

Figure 19. Longitudinal Girder Strain Across Span A

CONCLUSIONS

- ABAQUS has many modeling characteristics with which to model reinforced concrete.

- ABAQUS can to do the following:

  — model concrete and steel with beam and shell elements
  — simulate their interaction
  — apply loads
  — calculate accurate results and predict behavior not generally obtained through experimentation.

- The accuracy of the model was validated, and the limitations of matching finite element models to experimental tests held under conditions that are less than ideal was illustrated.

- The development of a finite element model of an entire bridge illustrates not only the capability of ABAQUS to represent the behavior of a realistic structure but also the specific capability of the model to predict deflections, strains, and stresses while minimizing unnecessary complexities.

RECOMMENDATION

- VDOT should consider implementing contemporary analysis tools such as ABAQUS.

REFERENCES

Alfaiate, J., Pires, E.B., & Martins, J.A.C. (1997). A Finite Element Analysis of Non-Prescribed Crack Propagation in Concrete. *Computers & Structures*, 63(1): 17-26.

Ashour, A.F., & Morley, C.T. (1993). Three-dimensional Nonlinear Finite Element Modeling of Reinforced-Concrete Structures. *Finite Elements in Analysis and Design*, 15: 43-55.

Azizinamini, A. (1994). Old Concrete Slab Bridges: Analysis. *ASCE Journal of Structural Engineering*, 120(1): 3305-3319.

Barzegar, F. (1994). Generating Reinforcement in FE Modeling of Concrete Structures. *ASCE Journal of Structural Engineering*, 120(5): 1656-62.

Barzegar, F., & Maddipudi, S. (1997). Three-Dimensional Modeling of Concrete Structures II: Reinforced Concrete. *ASCE Journal of Structural Engineering*, 123(10): 1347-1356.

Chen, W.-F., Yamaguchi, E., Kotsovos, M.D., & Pan, A.D. (1993). Constitutive Models. In *Finite Element Analysis of Reinforced-Concrete Structures II: Proceedings of the International Workshop*. New York: American Society of Civil Engineers, pp. 36-117.

Chowdhury, M.R. (1995). Further Considerations for Nonlinear Finite-Element Analysis. *Journal of Structural Engineering*, 121: 1377-1379.

Darwin, D. (1993). Reinforced Concrete. In *Finite Element Analysis of Reinforced-Concrete Structures II: Proceedings of the International Workshop.* New York: American Society of Civil Engineers, pp. 203-232.

DeBorst, R. (1997). Some Recent Developments in Computational Modeling of Concrete Fracture. *International Journal of Fracture*, 86(1-2): 5-36.

Gilbert, R., & Warner, R. (1978). Tension Stiffening in Reinforced-Concrete Slabs. *ASCE Journal of Structural Engineering*, 104: 1885-1900.

Graddy, J.C., Burns, N.H., & Klingner, R.E. (1995). *Factors Affecting the Design Thickness of Bridge Slabs.* (Report No. FHWA/TX-95+1305-3F). Center for Transportation Research, University of Texas at Austin.

Hibbitt, Karlsson & Sorensen, Inc. (1998a). *ABAQUS/Standard User's Manual; Version 5.8 (Vols. I-III)*. Rhode Island: Author.

Hibbitt, Karlsson & Sorensen, Inc. (1998b). *ABAQUS/Standard Update Manual: Example Problems, Verification, Theory; Version 5.8*. Rhode Island: Author.

Huria, V. (1993). Nonlinear Finite Element Analysis of RC Slab Bridge. *ASCE Journal of Structural Engineering*, 119(1): 88-107.

Jiang, J., & Mirza, F.A. (1997). Nonlinear Analysis of Reinforced-concrete Slabs by a Discrete Finite Element Approach. *Computers & Structures*, 65(4): 585-592.

Kwak, H.G., & Filippou, F.C. (1997). Nonlinear FE Analysis of RC Structures Under Monotonic Loads. *Computers & Structures*, 65(1): 1-16.

Loo, Y.C., & Guan, H. (1997). Cracking and Punching Shear Failure Analysis of RC Flat Plates. *ASCE Journal of Structural Engineering*, 123(10): 1321-1330.

Mabsout, M. (1997). Finite Element Analysis of Steel Girder Highway Bridges. *Journal of Bridge Engineering*, 2(3): 83-87.

Misch, P. (1998). Experimental and Analytical Evaluation of an Aluminum Deck Bridge. Postgraduate Thesis, University of Virginia, Charlottesville.

Ngo, D., & Scordelis, A.C. (1967). Finite Element Analysis of Reinforced-Concrete Beams. *Journal of the American Concrete Institute*, 65(9): 757-766.

Ramaswamy, A., Barzegar, F., & Voyiadjis, G.Z. (1995). Study of Layering Procedures in Finite Element Analysis of RC Flexural and Torsional Elements. *ASCE Journal of Structural Engineering*, 121(12): 1773-1783.

Razaqpur, A.G. (1990). Analytical Modeling of Nonlinear Behavior of Composite Bridges. *Journal of Structural Engineering*, 116: 715-1733.

Reed, A. (1996). The Alternatives for the Woodrow Wilson Bridge. *The Washington Post*, Article ID #9604110056, p. J03.

Scanlon, A., & Murray, D. (1974). Time-Dependent Reinforced-Concrete Slab Deflections. *ASCE Journal of Structural Engineering*, 100: 1911-1924.

Sen, R., Issa, M., Sun, X., & Gergess, A. (1994). Finite Element Modeling of Continuous Posttensioned Voided Slab Bridges. *ASCE Journal of Structural Engineering*, 120(2): 651-667.

Shahrooz, B.M. (1994). Nonlinear Finite Element Analysis of Deteriorated RC Slab Bridge. *ASCE Journal of Structural Engineering*, 120(2): 422-424.

Shahrooz, B.M., & Ho, I.K. (1998). Finite Element Modeling of a Deteriorated RC Slab Bridge: Lessons Learned and Recommendations. *Structural Engineering & Mechanics*, 6(3): 259-274.